INTERNATIONAL JOURNAL FOR NUMERICAL METHODS IN FLUIDS
Int. J. Numer. Meth. Fluids 2002; **40**:217–230 (DOI: 10.1002/fld.274)

A cascadic conjugate gradient algorithm for mass conservative, semi-implicit discretization of the shallow water equations on locally refined structured grids

Luca Bonaventura*,† and Giorgio Rosatti

Dipartimento di Ingegneria Civile ed Ambientale, Università degli Studi di Trento, Italy

SUMMARY

A semi-implicit, mass conservative discretization scheme is applied to the two-dimensional shallow water equations on a hierarchy of structured, locally refined Cartesian grids. Different resolution grids are fully interacting and the discrete Helmholtz equation obtained from the semi-implicit discretization is solved by the cascadic conjugate gradient method. A flux correction is applied at the interface between the coarser and finer discretization grids, so as to ensure discrete mass conservation, along with symmetry and diagonal dominance of the resulting matrix. Two-dimensional idealized simulations are presented, showing the accuracy and the efficiency of the resulting method. Copyright © 2002 John Wiley & Sons, Ltd.

KEY WORDS: cascadic conjugate gradient; multigrid; shallow water equations; semi-implicit schemes

1. INTRODUCTION

In many numerical models for environmental applications, semi-implicit time discretization is employed in order to improve computational efficiency. This approach has proven to be quite successful in areas such as coastal hydrodynamics and meteorological modelling (see e.g. References [1–4]). Semi-implicit time discretization leads to the formulation of a Helmholtz equation that must be solved numerically at each time step. Therefore, the computational burden of the semi-implicit step can rise significantly in high-resolution models and the use of highly efficient numerical solvers is mandatory to maintain overall efficiency of the semi-implicit approach.

Local refinement of the discretization grid can reduce the dimensions of the algebraic problem to be solved and enhance the resolution where the solution is expected to have larger gradients and more complex structure. Furthermore, many environmental applications are concerned with large-scale phenomena that interact with finer scale domain features. As

*Correspondence to: L. Bonaventura, Dipartimento di Ingegneria Civile ed Ambientale, Università degli Studi di Trento, Mesiano di Povo, 38050 TN, Italy.
†E-mail: bonavent@ing.unitn.it

Received May 2001
Revised September 2001

typical examples of such problems, one may consider, e.g. modelling the Venice Lagoon dynamics as fully coupled to the Adriatic Sea, or weather forecasting in Northern Italy when a synoptic low is impinging on the Alps. Unfortunately, the matrix resulting of straightforward finite difference/finite volume discretizations of the Helmholtz equation has a spectral condition number that grows like the ratio of the largest to the smallest cell volume in the discretization grid, as it can be shown directly by Gerschgorin's circle theorem (see e.g. Reference [5]). Thus, the convergence speed of standard iterative algorithms deteriorates rapidly.

In the present work, the cascadic conjugate gradient method (CCG) proposed by Deuflhard in References [6, 7] will be applied to the semi-implicit discretization of the shallow water equations in a multiple resolution framework. With this technique, for each refinement level an algebraic problem is solved for that level and all the coarser levels. This solution is used as initial guess to compute the solution on a grid hierarchy including the next refinement level. For locally refined grids, CCG can be interpreted as a kind of multilevel preconditioner that reduces effectively the high condition number of locally refined grids. It was shown in Reference [7] that CCG can be even more effective than other multilevel preconditioners (see e.g. Reference [8]). It was then proven in Reference [6] that this method achieves the same computational complexity as classical multigrid methods, while using solvers based on the conjugate gradient method. In the numerical scheme presented in this paper, the CCG technique is coupled to an appropriate treatment of the coarse/fine interface according to the technique proposed in Reference [9]. The resulting scheme for the shallow water equations is locally and globally mass conservative. Furthermore, a symmetric, positive definite and diagonally dominant matrix is inverted at each time step, using a solver with optimal computational complexity. A number of idealized test cases have been carried out with this numerical scheme, in order to assess its effective accuracy and computational cost. In all the tests, rather extreme cases of typical wave propagation phenomena were considered. In particular, the applicability of the method with time-independent grid refinement was studied, as it is the case for typical environmental models of regions with complex bathymetry/orography. Only very small interface effects were produced at the internal boundary between coarse and fine grids and correct solutions were obtained with time-independent grid refinement, even in cases with strong dynamical interaction of the different grids. The expected computational gain over standard conjugate gradient algorithms was clearly achieved, as well as the optimal scaling of the computational cost for a given accuracy with respect to the total number of gridpoints. Furthermore, the numerical scheme was able to reproduce correctly sharp features of the solution due to irregular bathymetry, although employing exactly the same spatial discretization at each hierarchy level.

Application of the cascadic approach to the problems reviewed above appears promising also because, for these applications, the large-scale dynamics of the coarser grids is essentially driving the finer grids. Thus, it will be advantageous to start the finer level iterations from the coarser grid solution. On the other hand, all the grids interact dynamically and no one-way nesting or nudging of the finer grids into the coarser are performed. Another important feature of the CCG approach is that no special care appears to be necessary to allow for irregular domains and strongly varying equation coefficients. This could be a possible advantage over the alternative choice with optimal computational complexity, i.e. multigrid itself. The multigrid method has been successfully applied to semi-implicit or pressure projection algorithms for domains with simple geometries also using locally refined or adaptive grids (see e.g. References [10–12]). However, in environmental problems such as coastal and

mesoscale modelling, the computational domain itself can be rather different at different resolutions. Bathymetry and orography are described by irregular functions that depend strongly on spatial resolution. Furthermore, if a conservative discretization of the continuity equation is required, the resulting Helmholtz equation has coefficients that depend on the free-surface elevation at each time step. A convergence theorem for elliptic equations with such irregular coefficients was proven in Reference [13] for a variant of classical multigrid. Thus, it is surely possible to apply multigrid to the environmental problems considered in this paper. On the other hand, special coarse grid operators had to be developed for application of multigrid techniques to problems with strongly varying coefficients in homogeneization theory (see e.g. References [14, 15]) and various problems are known to arise in multigrid applications to highly inhomogeneous grids (see e.g. Reference [16]). Systematic comparison of the effective accuracy and efficiency of different multigrid and multilevel techniques in such irregular cases is certainly desirable, but beyond the scope of this paper. In the numerical experiments performed, however, CCG appears to reproduce correctly sharp features of the solution without need for any *ad hoc* treatment of the irregular equation coefficients and source terms. Furthermore, the CCG technique for models with structured Cartesian grids allows for fast and efficient extension of existing codes in a multiresolution framework.

The cascadic conjugate gradient method will be briefly reviewed in Section 2. A multilevel algorithm for the semi-implicit discretization of the shallow-water equations employing the cascadic conjugate gradient on a hierarchy of discretization grids be will be presented in Section 3. A detailed description of the treatment of coarse/fine grid interfaces will be given in Section 4. Numerical results obtained on idealized test cases will be presented in Section 5.

2. THE CASCADIC CONJUGATE GRADIENT METHOD

The cascadic conjugate gradient method has been proposed by Deuflhard [7] and fully analysed by Bornemann and Deuflhard [6]. This approach to the solution of an elliptic problem is based on the construction of the solution in a hierarchy of nested finite-dimensional functional spaces $X_i,\ i=0,\ldots,l$. These spaces are associated to nested discretization grids, so that X_0 denotes the space associated to the coarsest grid and $X_i \subset X_{i+1},\ i=0,\ldots,l-1$. At each level i of the grid hierarchy, an approximate solution in X_i is computed by means of a conjugate gradient solver. This solution is then used as the starting point for the iterations on the subsequent level $i+1$. It was shown in Reference [6] that this type of algorithm has, for a given accuracy, the same computational complexity of the classical multigrid method, provided that the number of iterations performed at each level is controlled in an appropriate way. More specifically, an estimate of the discretization error at each level is employed, so as to stop the iterative method as soon as the error in the solution of the algebraic system is approximately the same as the discretization error. If this can be achieved, the computational cost of such a procedure is $O(N_l)$, where N_l is the number of gridpoints of the grid associated with the largest functional space X_l at the finest discretization level. The CCG algorithm can also been implemented in an adaptive fashion, so as to refine the grid according to some refinement criterion where more resolution is found to be necessary. In a theoretical framework, CCG has been applied to various types of elliptic problems (see e.g. References [17, 18]). Developments of the technique more specifically aimed at realistic applications with problems analogous to those outlined in Section 1 are presented in Reference [19].

3. MULTILEVEL SEMI-IMPLICIT DISCRETIZATION OF THE SHALLOW WATER EQUATIONS

The two-dimensional, vertically averaged shallow water equations can be written as

$$\frac{\partial U}{\partial t} + U\frac{\partial U}{\partial x} + V\frac{\partial U}{\partial y} = -g\frac{\partial \eta}{\partial x} - \gamma U \tag{1}$$

$$\frac{\partial V}{\partial t} + U\frac{\partial V}{\partial x} + V\frac{\partial V}{\partial y} = -g\frac{\partial \eta}{\partial y} - \gamma V \tag{2}$$

$$\frac{\partial \eta}{\partial t} + \frac{\partial (UH)}{\partial x} + \frac{\partial (VH)}{\partial y} = 0 \tag{3}$$

where U and V are the vertically averaged horizontal velocity components in the x and y directions, respectively, η is the free surface elevation with respect to an undisturbed water level, h is the bottom depth with respect to the same level, g is the acceleration of gravity and $\gamma = g\sqrt{(U^2 + V^2)}/\chi^2$, where χ is a friction coefficient and $H = h + \eta$ is the total water depth. The advective form is chosen for the momentum equation, while conservation of the fluid mass is required. In a typical semi-implicit discretization (see e.g. Reference [20]), the free-surface gradients in Equations (1) and (2) and the velocities in Equation (3) are discretized implicitly, while some explicit method is employed for the discretization of the advective terms (semi-Lagrangian schemes are among the most efficient choices for applications to advection-dominated flows, see e.g. Reference [21]). The unknown values of U^{n+1} and V^{n+1} are then substituted into the Crank–Nicholson implicit time discretization of Equation (3) in order to obtain a Helmholtz equation for the free-surface η, which can be written in the simplest case as

$$\eta^{n+1} - g\theta^2\Delta t^2\left[\frac{\partial}{\partial x}\left(\frac{H^n}{1+\gamma^n\Delta t}\frac{\partial}{\partial x}\eta^{n+1}\right) + \frac{\partial}{\partial y}\left(\frac{H^n}{1+\gamma^n\Delta t}\frac{\partial}{\partial y}\eta^{n+1}\right)\right] = \mathscr{F}^n \tag{4}$$

where all the explicit terms have been collected in the right-hand side $\mathscr{F}^n$. Here, θ is an implicitness parameter which is required to be larger than $\frac{1}{2}$ for stability. Once Equation (4) has been solved, the values of U^{n+1} and V^{n+1} are computed by direct substitution of η^{n+1} in the discretization of Equations (1) and (2). As previously remarked, Equation (4) has to be solved at each time step on rather irregular computational domains. In typical environmental applications the equation coefficients, the forcing and the resulting solution depend strongly on spatial resolution. In order to discretize these equations on a locally refined grid, a solver based on CCG has been developed for this type of problem, which is incorporated in a model that discretizes Equations (1)–(3) on a hierarchy G_i, $i = 0, \ldots, l$ of nested, structured Cartesian grids. Each grid is composed of square cells with C-grid staggering of the discrete variables. In principle, these grids can be changed in time according to some adapting criterion, but for the applications targeted at this stage, only time-independent grids will be considered. In order to guarantee local and global mass conservation and to obtain a discretization of Equation (4) on $\bigcup_{i=0}^{k} G_i$ whose associated matrix is symmetric, positive definite and diagonally dominant, the finite volume method is applied and a flux continuity condition is imposed at each coarse/fine grid interface along the lines of Reference [9]. A detailed description of the discrete fluxes

employed at coarse/fine interfaces is presented in Section 4. Numerical simulations presented in Section 5 also show that this interface treatment allows to avoid spurious wave reflection at the internal finer grid boundary.

For each time step n, the outline of the resulting multilevel discretization algorithm is the following:

1. compute all the explicit terms on all grids $G_i, i=0,\ldots,l$
2. solve Equation (4) on $\bigcup_{i=0}^{l} G_i$ by the CCG algorithm, i.e.
   - 2.1. solve the discretization of (4) on G_0 by the conjugate gradient method
   - 2.2. for $k=1,\ldots,l$, use the solution on $\bigcup_{i=0}^{k-1} G_i$ as initial guess for the conjugate gradient solution of the discretization of (4) on $\bigcup_{i=0}^{k} G_i$
3. for $i=l-1,\ldots,1$, obtain the values of η in the refined areas of G_i by averaging the corresponding values computed previously on G_{i+1}
4. update velocities on all grids $G_i, i=0,\ldots,l$.

4. TREATMENT OF COARSE/FINE GRID INTERFACES

The discretization of Equation (4) at the coarse/fine grid interfaces is an essential feature of the method developed in this paper. In order to ensure mass conservation and good matrix properties, the discretization approach described in Reference [9] for the Poisson equation is employed, which amounts to require continuity of the mass fluxes at the boundaries of cells along each coarse/fine grid interface. For simplicity, the resulting discretization is described here only in the case of an interface parallel to the y direction, so that only Equations (1) and (3) will be involved in the derivation. Furthermore, advective terms and friction can be omitted without loss of generality, thus resulting in the system

$$\frac{\partial U}{\partial t} = -g\frac{\partial \eta}{\partial x}, \quad \frac{\partial \eta}{\partial t} + \frac{\partial (UH)}{\partial x} = 0 \tag{5}$$

For interface cells like those in Figure 1, the straightforward discretization of the free-surface gradients yields $O(1/\Delta X)$ errors, where ΔX denotes the cell spacing on the coarse grid. The flux continuous correction proposed in Reference [9] can be extended to the present case as

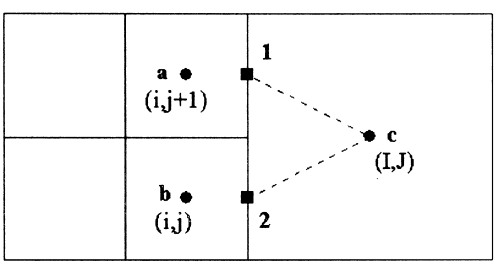

Figure 1. Interface between coarse and refined grid, from Reference [9].

follows. First, unknown free-surface values η_1, η_2 are introduced at points 1, 2, respectively. The flux per unit length on the left-hand side of the coarse/fine interface at point 1 is then computed as

$$F_\ell^1 = H_1 U_1 = H_1 \left(U_1^n - \frac{g\Delta t}{\Delta X/4}(\eta_1 - \eta_a) \right) = H_1 U_1^n - \frac{g\Delta t U_1}{\Delta X/4}(\eta_1 - \eta_a) \tag{6}$$

The corresponding flux on the right-hand side is computed as

$$F_r^1 = H_1 U_1 = H_1 \left(U_1^n - \frac{g\Delta t}{\Delta X/2}\left(\eta_c - \frac{\eta_1 + \eta_2}{2} \right) \right) \tag{7}$$

and continuity of the interface flux is imposed by requiring that $F_\ell^1 = F_r^1$, which yields the equation

$$\frac{g\Delta t H_1}{\Delta X/4}(\eta_1 - \eta_a) = \frac{g\Delta t H_1}{\Delta X/2}\left(\eta_c - \frac{\eta_1 + \eta_2}{2} \right) \tag{8}$$

The analogous equation can be written for point 2 and the unknown values η_1, η_2 can be computed as

$$\eta_1 = \tfrac{5}{6}\eta_a + \tfrac{1}{3}\eta_c - \tfrac{1}{6}\eta_b, \quad \eta_2 = \tfrac{5}{6}\eta_b + \tfrac{1}{3}\eta_c - \tfrac{1}{6}\eta_a$$

The flux $F_r^1 = F_\ell^1$ can then be computed by substitution of these values in (7), thus yielding

$$F_r^1 = H_1 U_1^n - \frac{2g\Delta t H_1}{3\Delta X}(2\eta_c - \eta_a - \eta_b) \tag{9}$$

The flux $F_r^2 = F_\ell^2$ can be derived analogously. From these formulas for the appropriate interface fluxes, the matrix coefficients for the interface cells can be derived. In the following, cell c on the coarse grid (see Figure 1) will be denoted by indexes (I,J), and in general all cells belonging to the coarse grid will be denoted by capital indexes, while the cells a, b, on the fine grid will be denoted by $(i, j+1)$ and (i,j), respectively. The discrete equation for the unknown value $\eta_{I,J}^{n+1}$ can be written as resulting from the finite volume discretization of (3),

$$\begin{aligned} \Delta X \Delta Y \eta_{I,J}^{n+1} = \Delta X \Delta Y \eta_{I,J}^n - \Delta t \left[\frac{\Delta Y}{2} F_{i+1/2,j} + \frac{\Delta Y}{2} F_{i+1/2,j+1} - \Delta Y F_{I,J+1/2} \right] \\ - \Delta t \Delta X [F_{I,J+1/2}^n - F_{I,J-1/2}] \end{aligned} \tag{10}$$

Rewriting the fine grid fluxes per unit length according to Equation (9) and assuming $\theta = 1$ for simplicity, by substitution in (10) one obtains

$$\begin{aligned} &\eta_{I,J}^{n+1}\left[1 + \frac{g\Delta t^2}{\Delta X^2}\frac{2}{3}(H_{i+1/2,j}^n + H_{i+1/2,j+1}^n) + \frac{g\Delta t^2}{\Delta X^2} H_{I+1/2,J}^n + \frac{g\Delta t^2}{\Delta Y^2} H_{I,J+1/2}^n + \frac{g\Delta t^2}{\Delta Y^2} H_{I,J-1/2}^n \right] \\ &- \eta_{i,j}^{n+1}\frac{g\Delta t^2}{\Delta X^2}\frac{1}{3}(H_{i+1/2,j}^n + H_{i+1/2,j+1}^n) - \eta_{i,j+1}^{n+1}\frac{g\Delta t^2}{\Delta x^2}\frac{1}{3}(H_{i+1/2,j}^n + H_{i+1/2,j+1}^n) \\ &- \eta_{I+1,J}^{n+1}\frac{g\Delta t^2}{\Delta X^2} H_{I+1/2,J}^n - \eta_{I,J+1}^{n+1}\frac{g\Delta t^2}{\Delta Y^2} H_{I,J+1/2}^n - \eta_{I,J-1}^{n+1}\frac{g\Delta t^2}{\Delta y^2} H_{I,J-1}^n = \delta_{I,J} \end{aligned} \tag{11}$$

where $\delta_{I,J}$ denotes the right-hand side containing all the explicit terms. The discrete equation for the unknown values $\eta_{i,j}^{n+1}, \eta_{i,j+1}^{n+1}$ can be derived analogously. Setting $\Delta x = \Delta X/2$, $\Delta y = \Delta Y/2$, one obtains

$$\eta_{i,j}^{n+1}\left[1+\frac{g\Delta t^2}{\Delta x^2}\frac{1}{3}H_{i+1/2,j}^n+\frac{g\Delta t^2}{\Delta x^2}H_{i-1/2,j}^n+\frac{g\Delta t^2}{\Delta y^2}H_{i,j+1/2}^n+\frac{g\Delta t^2}{\Delta y^2}H_{i,j-1/2}^n\right]$$
$$-\eta_{I,J}^{n+1}\frac{g\Delta t^2}{\Delta x^2}\frac{2}{3}H_{i+1/2,j}^n-\eta_{i-1,j}^{n+1}\frac{g\Delta t^2}{\Delta x^2}H_{i-1/2,j}^n$$
$$-\eta_{i,j+1}^{n+1}\left(-\frac{g\Delta t^2}{\Delta y^2}H_{i,j+1/2}^n+\frac{g\Delta t^2}{\Delta x^2}\frac{1}{3}H_{i+1/2,j}^n\right)-\eta_{i,j-1}^{n+1}\frac{g\Delta t^2}{\Delta y^2}H_{i,j-1}^n=\delta_{i,j} \tag{12}$$

$$\eta_{i,j+1}^{n+1}\left[1+\frac{g\Delta t^2}{\Delta x^2}\frac{1}{3}H_{i+1/2,j+1}^n+\frac{g\Delta t^2}{\Delta x^2}H_{i-1/2,j+1}^n+\frac{g\Delta t^2}{\Delta y^2}H_{i,j+3/2}^n+\frac{g\Delta t^2}{\Delta y^2}H_{i,j-3/2}^n\right]$$
$$-\eta_{I,J}^{n+1}\frac{g\Delta t^2}{\Delta x^2}\frac{2}{3}H_{i+1/2,j+1}^n-\eta_{i-1,j+1}^{n+1}\frac{g\Delta t^2}{\Delta x^2}H_{i-1/2,j+1}^n$$
$$-\eta_{i,j}^{n+1}\left(-\frac{g\Delta t^2}{\Delta y^2}H_{i,j+1/2}^n+\frac{g\Delta t^2}{\Delta x^2}\frac{1}{3}H_{i+1/2,j+1}^n\right)-\eta_{i,j+2}^{n+1}\frac{g\Delta t^2}{\Delta y^2}H_{i,j+2}^n=\delta_{i,j+1} \tag{13}$$

As in Reference [9], some conditions at the coarse/fine grid interface must be required, in order to achieve a system of equations for the unknowns η^{n+1} on the refined grid that is symmetric, positive definite and diagonally dominant. By direct inspection of Equations (11)–(13) it is easy to see that, for symmetry to hold, the condition

$$H_{i+1/2,j}^n = H_{i+1/2,j+1}^n = H_{I-1/2,J}^n$$

must be required, which can be interpreted as a consistency requirement for the total fluid depths at the coarse/fine interface. This condition is easy to enforce and does not imply any restriction on the practical applicability of the resulting semi-implicit scheme. Another condition involving the fluid depths results from imposing strict diagonal dominance of the refined grid matrix, which requires the coefficient of $\eta_{i,j+1}^{n+1}$ in Equation (12) and the corresponding coefficient of $\eta_{i,j}^{n+1}$ in Equation (13) to be negative, thus yielding in the condition

$$H_{i+1/2,j}^n > 3\frac{\Delta x^2}{\Delta y^2}H_{i,j+1/2}^n$$

This inequality must hold along all the coarse/fine interfaces. If a unity cell aspect ratio is assumed, this condition is easily satisfied in typical applications of shallow water models to atmospheric flows or coastal hydrodynamics. The only obvious exception are those very shallow areas where wetting/drying of computational cells may occur and shallow flats at the very edge of much deeper channels. If care is taken in the grid refinement strategy to avoid placing refinement interfaces in these quite peculiar areas, this condition is automatically satisfied and does not pose any restriction on the applicability of the numerical scheme.

5. NUMERICAL EXAMPLES

Numerical tests have been carried out in idealized test cases in order to assess the accuracy, efficiency and robustness of the algorithm described in Section 3. Semi-implicit time discretization was performed along the lines outlined above for the equations:

$$\frac{\partial U}{\partial t} = -g\frac{\partial \eta}{\partial x} - \gamma U + F_u \tag{14}$$

$$\frac{\partial V}{\partial t} = -g\frac{\partial \eta}{\partial y} - \gamma V + F_v \tag{15}$$

$$\frac{\partial \eta}{\partial t} + \frac{\partial (UH)}{\partial x} + \frac{\partial (VH)}{\partial y} = F_\eta \tag{16}$$

Here, the advection terms have been neglected and non-homogeneous terms have been included, so that arbitrary functions U, V and η can be assigned as the analytic solution of Equations (14)–(16) by specifying appropriate non-zero F_u, F_v and F_η. The results of tests on the non-homogeneous equations with known analytic solution are presented in Section 5.1, while in the other cases the forcing was assumed to be zero. It is to be remarked that all the tests performed were aimed at understanding the model response in rather extreme cases of wave propagation phenomena. In this way, the reliability of the model for potential applications to shallow-water problems can be assessed. The numerical experiments have focussed especially on the purely numerical effects resulting from large-scale dynamical features crossing time-independent coarse/fine boundaries. In fact, time-independent grid refinement would be the rule in applications over complex bathymetries and absence of relevant spurious interface effects is essential for the applicability of the method. A CCG solver was employed at each time step to produce the solution on a hierarchy of uniform grids.

In order to mimic the typical setting of the applications targeted for use of this model, the computational domain was represented by a box of sides $L_x = L_y = 10$ km long. At the boundaries, the mass flux was assumed to be zero as well as the normal velocity components. In most of the tests, a hierarchy of 4 refinement patches was considered, with sides length of 5, 2.5, 1.25 km, respectively. The locally refined patches zoom down on the domain centre. The spatial discretization step at the coarsest level was assumed to be $\Delta x^{(1)} = \Delta y^{(1)} = 500$ m. The resolution was then doubled at each refinement level, thus leading to $\Delta x^{(4)} = 62.5$ m for the finest grid. The implicitness parameter was in general taken to be $\theta = 0.52$. The CCG solver was equipped with a simple implementation of the hierarchic termination criterion proposed in Reference [6], where it was shown that use of such a criterion is essential in order to achieve optimal operation count. According to this termination criterion, a tolerance ε_1 is prescribed for terminating the CCG at the coarsest level $k = 1$ at reasonable accuracy. The tolerance for each level $k = 2, \ldots, l$ is then given recursively by

$$\varepsilon_k = \varepsilon_{k-1} + E_{k-1}\rho\|\eta\| \left[\frac{\varepsilon_{\mathrm{CGG}}}{E_{k-1}} \left(\frac{N_k}{N_{k-1}} \right)^{1/d} \right]^{(d+1)/2}$$

Here, d is the number of space dimensions of the elliptic problem that is being discretized, $\|\eta\|$ is the magnitude of the solution in the energy norm induced by the elliptic operator,

$\rho \in (0,1)$ is a safety factor, N_k is the dimension of the discrete space X_k associated to the discretization level k, $\varepsilon_{\mathrm{CCG}}$ is the relative accuracy that is required for the solution on the largest discretization space X_l and E_k is an estimate of the relative approximation error for the discretization of the elliptic operator in X_k. In all the tests performed here, $\varepsilon_{\mathrm{CCG}} = 10^{-5}$ and $\varepsilon_1 = 10^{-9}$, while the safety factor was given to be by $\rho = 0.3$. The relative error was very roughly estimated by $E_k \approx (\Delta x^{(k)})^2$ and $\|\eta\| \approx L_x^{d/2}$. Furthermore, at each level $k = 1, \ldots, l$ the resulting tolerance ε_k was rescaled with the norm of the right-hand side of the linear system to be solved. Although extremely simplified and only heuristically based, this implementation of the termination criterion was found to be effective in order to achieve the theoretical estimate for the computational cost of the CCG solver, see e.g. Figure 4. Use of more appropriate and more accurate estimates of the space and time-discretization error (see e.g. Reference [22]) would be advisable for a more general and robust implementation of the CCG solver.

5.1. Analytic solutions of the inhomogeneous equations

In order to estimate the discretization error of the proposed method, the solution of Equations (14)–(16) was taken to be given by $U = U_0 \sin(\omega t) \sin^2(2\pi x/L_x) \cos(2\pi y/L_y)$, $V = V_0 \sin(\omega t) \sin^2(2\pi y/L_y) \cos(2\pi x/L_x)$, $\eta = \eta_0 + \eta_1 \cos(\omega t) \cos^2(2\pi x/L_x) \cos^2(2\pi y/L_y)$. The lengthy expressions of the appropriate F_η, F_u, and F_v are omitted here. h and γ were taken to be equal to zero. Clearly, local refinement does not make much sense for such a low wavenumber solution pattern. However, the aim of the test is to show that the interface treatment does not introduce extra discretization errors in a most unfavourable case. If the same test is repeated with solutions that have sharp peaks in the refined grids, the expected significant error reduction is observed. The values $\eta_0 = 5\,\mathrm{m}$ and $\eta_1 = 0.5\,\mathrm{m}$ were prescribed for the reference sea level and amplitude of the free-surface oscillations, along with $U_0 = V_0 = 1\,\mathrm{m\,s^{-1}}$. This results in a maximum value of $\sqrt{gH} = 7.35\,\mathrm{m\,s^{-1}}$ for the gravity wave celerity. The frequency was given to be by $\omega = 1.775 \times 10^{-3}\,\mathrm{s^{-1}}$, which corresponds to an oscillation period T of about 1 h. The time step was taken to be $\Delta t = T/40 = 90\,\mathrm{s}$, thus resulting in maximum one-dimensional Courant numbers $(\sqrt{gH}\Delta t)/\Delta x^{(4)} = 10.58$, $(U_0 \Delta t)/\Delta x^{(4)} = 1.44$, respectively. The behaviour of the resulting l_∞ and l_2 absolute errors with respect to the analytic solution for the free-surface elevation are displayed in Figure 2. These errors were computed in a $10T$ long run on the variable resolution computational grid. The errors on the computed values of η have comparable values in the two error norms, thus hinting that rather uniformly distributed errors arise, while the errors on velocity appear to be more localized. It can be observed that, in spite of the rather extreme features of the solution, the l_∞ error always remained below 2 cm, which is just above the typical magnitude of tidal gauge errors.

The l_∞ absolute errors for the free-surface elevation are compared in Figure 3 to the l_∞ errors of the corresponding computation performed with the same time step on a single uniform resolution grid with $\Delta x = \Delta x^{(1)}$. It can be observed that, for this low wavenumber solution, the dominant error component in the computation on the multilevel hierarchy is due to the coarsest grid level. On the other hand, no $O(1/\Delta x^{(i)})$ errors arise as a result of the appropriate interface treatment. This test in which a known analytic solution is available was also used to estimate the CCG solver performance and compare it to the performance of a standard preconditioned conjugate gradient (PCG) solver. For the comparison, a simple PCG solver with diagonal preconditioning was employed, which performs very efficiently on uniform grids. In Figure 4 the normalized computational cost $C_l = (\sum_{i=1}^{l} I_i N_i)/N_l$, of a CCG matrix inversion

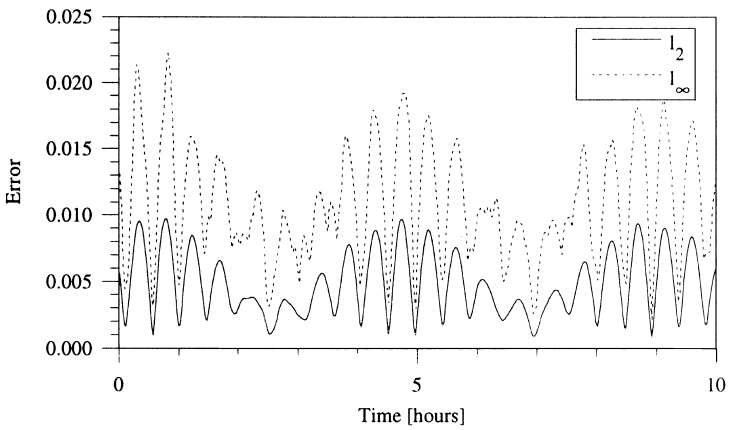

Figure 2. l_∞ and l_2 errors with respect to the analytic solution for the free-surface elevation on the 4 levels grid hierarchy.

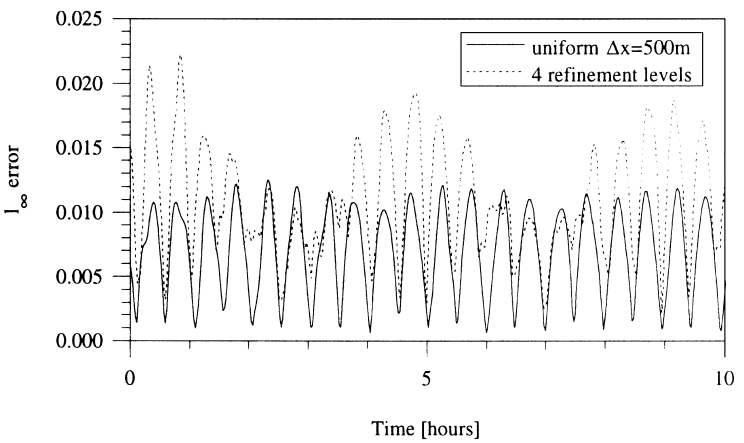

Figure 3. l_∞ errors for the free-surface field on the coarsest grid vs errors on the 4 levels grid hierarchy.

is displayed for computations on grid hierarchies with 1–5 levels. Here, I_k denotes the number of iterations of the CCG solver on $\bigcup_{i=0}^{k} G_i$ and N_k the number of gridpoints of the same grid. The number of iterations is averaged over a large number of timesteps in order to account for the time evolution of the solution pattern. As a comparison, the number of iterations for a standard PCG solver on the same grid hierarchy is also shown. The analytic solution was used in order to compare iteration counts that lead to approximately equal errors in the solution. It can be seen that the two comparable indicators of computational cost differ substantially already with 3 refinement levels. For 4 refinement levels, the computational cost of PCG is more than double of CCG. For 5 refinement levels PCG essentially does not converge any more, even if a maximum iteration number above 2000 is allowed. Furthermore, it can be

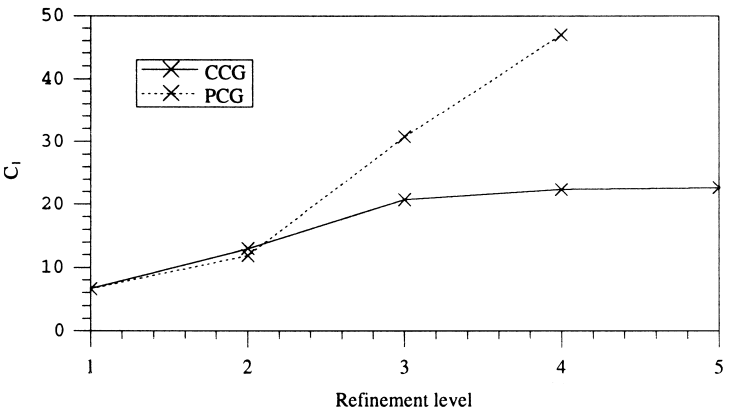

Figure 4. Computational cost C_l of CCG solver on multilevel hierarchies, normalized with number of gridpoints.

observed that the computational cost C_l of CCG is approximately constant, according to the theoretical estimates of Reference [6].

5.2. Outcoming waves

In order to show how the discretization algorithm outlined in Section 3 allows for full dynamical interaction between the grids at various resolutions, without any relevant spurious effects at the grid interfaces, propagation of a strong gravity wave was simulated in the square closed basin described above. The initial datum for the free surface was given by $\eta = \eta_0 + \eta_1 \cos^2(\pi d(x, y)/(2\sigma))$, where $d(x, y) = \sqrt{(x - L_x/2)^2 + (y - L_y/2)^2}$, $\eta_0 = 20$ m, $\eta_1 = 2$ m and $\sigma = 1500$ m were prescribed. The bathymetry and the initial velocities were taken to be zero, while the Chézy friction coefficient was taken to be $\chi = 50\ \mathrm{m}^{1/2}\ \mathrm{s}^{-1}$. The time step used was $\Delta t = 10$ s, which amounted to a maximum one-dimensional Courant number $(\Delta t/\Delta x^{(4)})\sqrt{gH} = 2.35$. In Figure 5(a), the free-surface elevation is shown as computed on the coarsest grid of the 4 levels grid hierarchy at time $t = 200$ s, while in Figure 5(b) the same result is shown as computed at the same time on the grid at refinement level 3. It is to be reminded here that, in all the tests, the values of η in the refined areas of a level i grid are obtained at each time step by averaging the values on the corresponding 4 cells at level $i + 1$. It can be seen that the wave is free to propagate through the various discretization grids and that no spurious wave reflection takes place at the grid interfaces. No analytic solution is available in this case, but the computed solution compares well with the solutions obtained on a single grid at either the coarsest or the finest resolution, shown in Figures 5(c) and 5(d), respectively. Furthermore, it can be observed that the main wave travels at the correct speed $\sqrt{gH}$, where H is taken to be the total fluid depth at the initial time.

5.3. Free oscillations over rough bathymetry

In order to check the robustness of the model in handling rough bathymetries, free oscillations were computed in the case of free oscillations over a very steep bathymetry profile. As remarked in Section 1, it will be seen that the local grid refinement does in fact allow to

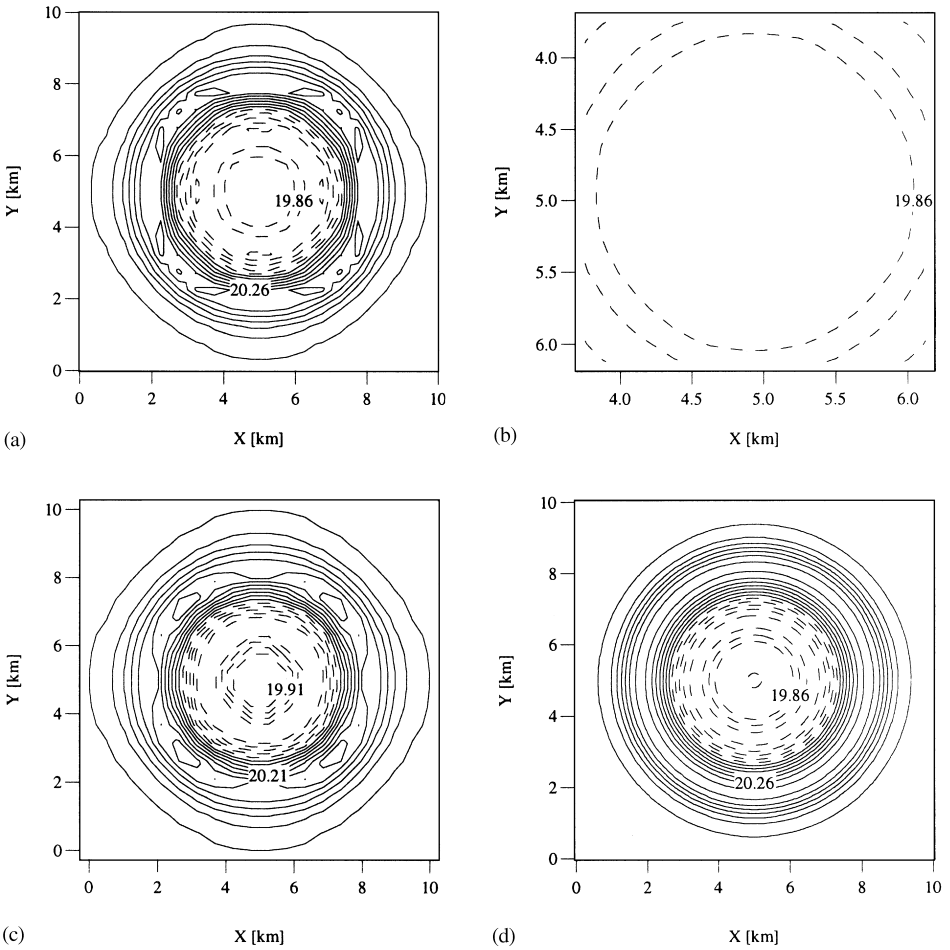

Figure 5. Free-surface elevation at time $t=200$ s computed on: (a) coarsest grid of 4 level hierarchy, (b) grid at third refinement level, (c) single grid at resolution $\Delta x^{(1)}$, (d) single grid at resolution $\Delta x^{(4)}$. Contour intervals of 5 cm.

reproduce small scale phenomena that are unresolved on the coarse grid. This is achieved without introducing *ad hoc* spatial discretizations on the coarser grids. The bathymetry was given by the function $h(x,y)=h_0-h_1\cos^2(\pi d(x,y)/(2\sigma))$, where

$$d(x,y)=\sqrt{(x-L_x/2)^2+(y-L_y/2)^2},$$

$h_0=0$, $h_1=5.3$ m $\sigma=1000$ m. It can be observed that the support of this function is only $2\Delta x^{(1)}$ wide on the coarsest grid, while it is $16\Delta x^{(4)}$ on the finest. The initial value for η was given by $\eta=\eta_0+\eta_1 x+\eta_1 y$, where $\eta_0=5$ m, $\eta_1=5/L_x=5/L_y$, while the initial velocities were taken to be zero and the Chézy friction coefficient was taken to be $\chi=50\ \mathrm{m}^{1/2}\ \mathrm{s}^{-1}$. Furthermore, the smallest total fluid depth on the coarsest grid at the initial time is about

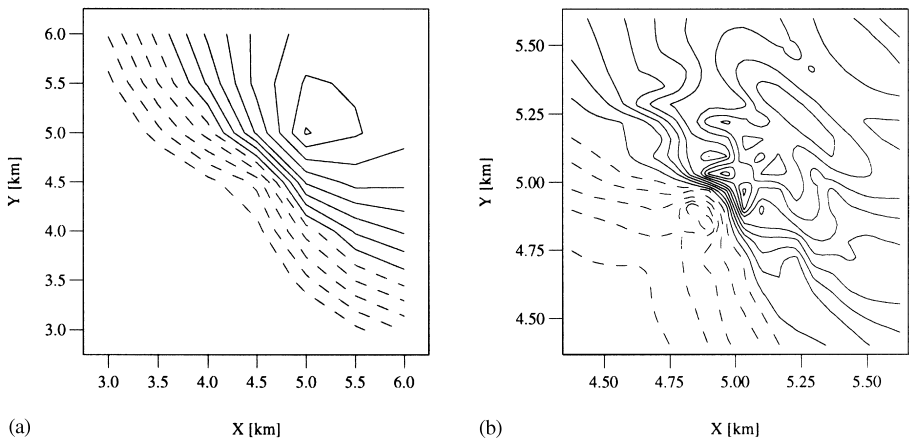

Figure 6. Free oscillations over steep bathymetry, free-surface computed at time $t=2000$ s on: (a) coarsest grid of 4 level hierarchy, (b) finest grid of 4 level hierarchy. Contour intervals of 6.5 cm.

35 cm, while on the finest a tiny island emerges, represented by a few gridpoints on top of the peak. The time step used was $\Delta t=20$ s, which amounted to maximum one-dimensional Courant numbers $(\Delta t/\Delta x^{(4)})\sqrt{gH}=2.24$, $(\Delta t/\Delta x^{(4)})U=0.64$, respectively. In Figure 6(a), a detail of the free-surface elevation field is displayed, as computed on the coarsest grid at time 2000 s. In Figure 6(b), the same result is shown as computed on the finest grid. At this time a large-scale wave has just swept over the tiny island and surface gravity waves in the lee of the peak can be observed, which are completely unresolved on the coarsest grid, thus showing that this type of approach is, in fact, robust enough to handle rough bathymetries.

6. CONCLUSIONS AND FUTURE DEVELOPMENTS

The cascadic conjugate gradient method has been applied to the Helmholtz equation obtained in semi-implicit discretizations of the shallow-water equations. It has been shown how CCG can be efficiently incorporated into a model for the solution of the shallow-water equations on a multilevel grid hierarchy. The resulting numerical scheme allows to achieve full dynamical interaction of all the refinement levels, as well as local and global mass conservation on the locally refined grid. The accuracy and efficiency of the resulting method were tested in a number of idealized wave propagation test cases. Further work is necessary in order achieve an optimal stopping criterion for the application of CCG to time dependent problems, but a simple implementation of the criterion proposed by Bornemann and Deuflhard has been shown to be sufficient to obtain great performance improvements with respect to standard conjugate gradient solvers. A two-dimensional multilevel shallow-water model employing the techniques outlined is currently under development for applications to river hydraulics, as well as long term simulations of pollutant and sediment transport in the Venice Lagoon. The CCG approach will also be applied to the semi-implicit discretization of fully compressible atmospheric models for mesoscale weather forecasting. In all these cases, models using CCG

on a hierarchy of structured Cartesian grids can be developed with modest programming overhead from previously existing models.

ACKNOWLEDGEMENTS

We would like to thank Luca Pavarino for the reference to the work of Bornemann and Deuflhard. Many stimulating discussions on multiple resolution models with Dieter Eppel and Hartmut Kapitza are gratefully acknowledged, as well as the constructive comments of Reinhold Hess and of two anonymous reviewers on a previous version of this paper.

REFERENCES

1. Casulli V. A semi-implicit finite difference method for nonhydrostatic, free surface flow. *International Journal for Numerical Methods in Fluids* 1999; **30**:425–440.
2. Casulli V, Cattani E. Stability, accuracy and efficiency of a semi-implicit method for three-dimensional shallow water flow. *Computers and Mathematics with Applications* 1994; **27**:99–112.
3. Côté J, Gravel S, Méthot A, Patoine A, Roch M, Stainforth A. The operational CMC-MRB global environmental multiscale (GEM) model, Part I: considerations and formulations. *Monthly Weather Review* 1998; **126**: 1373–1418.
4. Temperton C, Hortal M, Simmons A. A two-time-level semi-lagrangian global spectral model. *Quarterly Journal of the Royal Metereological Society* 2001; **127**:111–127.
5. Stoer J, Bulirsch R. *An introduction to Numerical Analysis* (2nd edn). Springer: New York/Berlin, 1980.
6. Bornemann FA, Deuflhard P. The cascadic multigrid method for elliptic problems. *Numerische Mathematik* 1996; **75**:135–152.
7. Deuflhard P. Cascadic conjugate gradient methods for elliptic partial differential equations: algorithm and numerical results. *Contemporary Mathematics* 1994; **180**:29–42.
8. Bramble JH, Pasciak JE, Xu J. Parallel multilevel preconditioners. *Mathematics of Computation* 1990; **55**:1–22.
9. Edwards MG. Elimination of adaptive grid interface errors in the discrete cell centered pressure equation. *Journal of Computational Physics* 1996; **126**:356–372.
10. Almgren A, Bell JB, Colella P, Howell LH, Welcome ML. A conservative adaptive projection method for the variable density incompressible Navier–Stokes equation. *Journal of Computational Physics* 1998; **142**:1–46.
11. Barros SRM. Multigrid methods for 2-dimensional and 3-dimensional poisson-type equations on the sphere. *Journal of Computational Physics* 1991; **92**:313–348.
12. Hess R. Dynamically adaptive multigrid on parallel computers for a semi-implicit discretization of the shallow water equations. *Technical Report 9/1999*, GMD, 1999.
13. Bramble JH, Pasciak JE, Wang J, Xu J. Convergence estimates for multigrid algorithms without regularity assumptions. *Mathematics of Computation* 1991; **57**:23–45.
14. Engquist B, Luo E. New coarse grid operators for highly oscillatory coefficient elliptic problems. *Journal of Computational Physics* 1996; **129**:296–306.
15. Moulton JD, Dendy Jr JE, Hyman JM. The black box multigrid numerical homogenization algorithm. *Journal of Computational Physics* 1998; **142**:80–108.
16. Pierce NA, Giles MB. Preconditioned multigrid methods for compressible flow calculations on stretched meshes. *Journal of Computational Physics* 1997; **136**(2):425–455.
17. Braess D, Dahmen D. A cascading multigrid algorithm for the stokes equations. *Numerische Mathematik* 1999; **82**:179–191.
18. Timmermann G. A cascadic multigrid algorithm for semilinear elliptic-problems. *Numerische Mathematik* 2000; **86**:717–731.
19. Lackner K. Menikoff R. Multiscale linear solvers for very large systems derived from PDEs. *SIAM Journal on Scientific Computing* 2000; **21**:1950–1968.
20. Casulli V. Semi-implicit finite difference methods for the two-dimensional shallow water equations. *Journal of Computational Physics* 1990; **86**:56–74.
21. Staniforth A, Cote J. Semi-lagrangian integration schemes for atmospheric models: a review. *Monthly Weather Review* 1991; **119**:2206–2223.
22. Houston P, Mackenzie JA, Suli E, Warnecke G. A posteriori error analysis for numerical approximations of friedrichs systems. *Numerische Mathematik* 1999; **82**:433–470.

